IEEE Access
Multidisciplinary | Rapid Review | Open Access Journal

Received February 26, 2020, accepted March 9, 2020, date of publication March 12, 2020, date of current version March 23, 2020.

Digital Object Identifier 10.1109/ACCESS.2020.2980371

Disturbance Observer-Based Finite-Time Speed Control for Marine Diesel Engine With Input Constraints

XUEMIN LI, YUFEI LIU, JIAN ZHANG, AND RUNZHI WANG
College of Power and Energy Engineering, Harbin Engineering University, Harbin 150001, China

Corresponding author: Jian Zhang (zhang_jian@hrbeu.edu.cn)

This work was supported in part by the National Natural Science Foundation of China under Grant 61803114, and in part by the Fundamental Research Funds for Central Universities under Grant 3072019CFM0301.

ABSTRACT In this article, a finite-time observer-based speed control strategy for the marine diesel engine is proposed with consideration of system parameter uncertainties, external disturbances and input constraints. Initially, a finite-time disturbance observer is designed, by which the synchronized uncertainties are accurately estimated in the sense of finite-time stability. Based on the observed information, a speed control strategy is proposed, and practical finite-time stability of the closed-loop system is demonstrated by rigorous theoretical analysis. Besides, for solving the input constraints inherent with the speed control system, an auxiliary variable is introduced to compensate the extra part of control output signals. Finally, numerical simulation and comparison are presented. The common operation situations of the marine diesel engines are taken into account, including starting, acceleration and deceleration between speed set points, sudden load changing, varied propulsion system parameters and different slope limits, etc. Comparing with the related existing method, the effectiveness and advantages of the proposed finite-time observer-based control law are illustrated.

INDEX TERMS Finite-time control, disturbance observer, input constraints, marine diesel engine.

I. INTRODUCTION

Diesel engines are extensively used as main engines and electric generators in ship industry by virtue of high thermal efficiency, reliable performance, and economic advantages [1]. When diesel engine is employed as marine main engine, the speed control of the engine is crucial for guaranteeing smooth cruise, since engine speed directly effects on the ship sailing speed [2]. Therefore, diesel engine speed control has been widely investigated in recent years. However, new challenges came up due to the application of new technologies such as exhaust gas recirculation (EGR) [3], hybrid propulsion [2], variable geometry turbocharger (VGT) [4], etc., which made the speed control more complicated and brought higher requirements for the entire engine system. Meanwhile, the actuators of speed control system also get improved, i.e. the traditional fuel pump rack has been substituted by high pressure common rail (HPCR) system. Thus it is possible to conduct control signals more precisely, because the HPCR performs accurate and flexible fuel injection. Therefore, advanced control algorithms can be applied to speed control system to further improve the marine diesel engine performance. Consequently, increasing research interest has been aroused in this field and extensive studies are reported on engine speed control strategies, see [5]–[13], and the references therein. As a simple and reliable control method, Proportion-Integration-Differentiation (PID) is commonly adopted to diesel engine speed control system [5]. Besides, fuzzy PID [6], H∞ PID [7], and PID controller combined with genetic algorithm [8] are investigated. In [12], a multi-sliding surface control scheme is proposed, different sliding surfaces are selected with consideration of the various engine working conditions.

However, it is noticeable that the existing control methods concerned with diesel engine speed control system can only achieve asymptotical stable property, which implies the convergence rate is at best exponential with infinite settling time. Meanwhile, due to the faster response speed, higher accuracy and better robustness, finite-time control laws have been a hot topic. In [14], the homogenous system theory is applied to

The associate editor coordinating the review of this manuscript and approving it for publication was Ning Sun.

study finite-time control problem for soft landing on asteroid, numerical simulation results show that the proposed method shows faster convergence rate and better disturbance rejection properties than the asymptotically stable controller. In [15], a finite-time consensus law is developed for multi-robot system by using terminal sliding mode control. For further enhancing system robustness, the unknown disturbances and system uncertainties should be properly compensated by the control strategies, thus adaptive mechanism [16], sliding mode control method [17], and neural network [18] have been adopted. Recently, observer-based control method has become a valid measure for estimating unknown information of the concerned system [19]–[23]. In [20], a homogenous observer is developed to estimate system states and output-feedback control law is achieved by adding a power integrator technique. In [21], a reduced-order disturbance observer is proposed to attenuate the uncertain disturbances in a class of continuous non-linear systems. It is noticeable that the observer technique is also upgraded by combining the finite time control approach [24]–[26]. In [24], a continuous finite-time extended state observer is presented to estimate the actuator faults and system uncertainties. In [25], a finite-time disturbance observer is first designed to reject the load disturbances variation, and then non-singular terminal sliding mode controller is proposed on basis of the observation information. By now, finite-time observer-based control has become an effective approach for stabilizing systems with unknown disturbance and uncertainties. Notably, the application of finite-time control methods and observer techniques would potentially improve engine speed control system performance, which is worthwhile to be studied.

In addition, finite-time control laws always demonstrate large control output signals to generate fast convergence rate, which inevitably results in large magnitude of system states. Nevertheless, state constraints [27]–[29] and actuator constraints such as input saturation [30], [31] and deadzone [32], [33] problem exist in practical system. Barrirer Lyapunov function (BLF) is employed to restrain the system states and control input simultaneously, and better tracking effect is guaranteed [28]. In [30], a nonlinear controller is first designed to handle input saturations and velocity feedback unavailability for the dual rotary crane system. In [31], an auxiliary system is introduced to solve non-symmetric saturation nonlinearity. In [33], actuator deadzone is considered in an articulated manipulator control system, and a finite-time controller is proposed. Considering the marine diesel engine, it is necessary to limit the fuel supply based on the operating condition, such that the economical efficiency is improved and the polluted emission is reduced [34]. Meanwhile, for engine speed control system, the fuel injectors in each cylinder is used as the main actuators, which inject certain mass of fuel into cylinder according to the control signals. Therefore, only positive control signals will be effectively reacted by the fuel injectors. By now, such practical problem have been received little attention among the related research works.

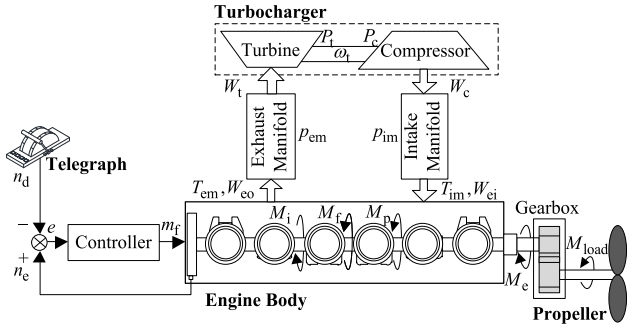

FIGURE 1. Schematic diagram of the marine diesel engine for propulsion.

Hence, the investigation of input constraints for engine speed control system is a meaningful topic with practical sense.

Given the challenges stated above, this work develops finite-time disturbance observer and finite-time controller for diesel engine speed control system in the presence of input constraints. The main achievements of the proposed control strategy are shown as follows: 1) Model deviations and external disturbances of the speed control system are summarized as synchronized uncertain term, which is estimated by the proposed finite-time disturbance observer. Afterwards, the estimated information is used to facilitate the control law design. 2) Due to the actuators of the speed control system only respond to positive signals, input constraints problem is explicitly handled in this paper. A finite-time control law is constructed by employing an auxiliary variable to overcome the input constraints.

The main contents of the following sections are given as follows. In Section 2, the mathematical model and the control objective of diesel engine speed control system are addressed. In Section 3, a finite-time disturbance observer is developed, then a finite-time control law with input constraints is further derived with the observed information. In Section 4, simulated works are carried out, effectiveness of the disturbance observer-based finite-time control law is verified, and comparison has been exhibited to show the superior performance of the proposed control scheme. Finally, the conclusion about the work is summarized, and further research of this paper is discussed in Section 5.

II. PRELIMINARIES

In Fig. 1, the schematic diagram of a marine diesel engine is presented, which is composed of the engine body, turbocharger, exhaust manifold and intake manifold. Additionally, aimed at speed control system analysis, a telegraph and a propeller are connected to the engine. Specifically, the telegraph provides a reference speed signal to the control system and load torque is acted on the engine by the propeller. The mathematical models and problem formulation will be illustrated in the following context. Then, some useful definitions and lemmas are given to facilitate the control scheme design.

A. MEAN VALUE ENGINE MODEL FOR DIESEL ENGINE

The mean value engine model (MVEM) is the most widely used control-oriented model for diesel engine by virtue of its easy implementation and high calculation speed [35] which is introduced for investigating the speed control strategy of diesel engine. In order to study the characteristics of the speed control system of marine diesel engine, mean value torque models of thermodynamic and kinetic processes will be addressed in detail, including the torque produced by fuel combustion, and the various internally and externally consumed torque.

Let M_{i} be the gross indicated torque stems from the fuel combustion in each cylinder, which is calculated as

$$M_{\mathrm{i}} = \frac{m_{\mathrm{f}} q_{\mathrm{LHV}} \eta_{\mathrm{i}} N_{\mathrm{cyl}}}{2\pi N_{\mathrm{st}}}, \tag{1}$$

where m_{f} is fuel mass injected into each cylinder per cycle, η_{i} is the gross indicated efficiency, q_{LHV} denotes the low heating value of diesel, N_{cyl} is the number of cylinders. N_{st} depends on the type of diesel engine, which takes 1 and 2 for a two-stroke engine and a four-stroke engine, respectively.

Note that during the working process, the indicated torque M_{i} is partially consumed internally, i.e. friction torque M_{f} and pumping torque M_{p} should be taken into consideration. Generally, M_{f} and M_{p} are calculated by empirical formulas. Here, M_{f} is assumed to be a quadratic polynomial of engine speed [36], and M_{p} is calculated based on the intake and exhaust manifold pressures as follows

$$M_{\mathrm{f}} = \frac{V_{\mathrm{d}}}{4\pi} 10^5 \left(k_1 n_{\mathrm{e}}^2 + k_2 n_{\mathrm{e}} + k_3\right) \tag{2}$$

$$M_{\mathrm{p}} = \frac{V_{\mathrm{d}}}{4\pi} \left(p_{\mathrm{em}} - p_{\mathrm{im}}\right) \tag{3}$$

where V_{d} denotes the total displacement, n_{e} is the engine speed, p_{em} and p_{im} respectively present the exhaust manifold pressure and the intake manifold pressure, k_1, k_2, k_3 are the experimental coefficients.

Thus, the effective torque generated by the marine diesel engine M_{e} is obtained

$$M_{\mathrm{e}} = M_{\mathrm{i}} - M_{\mathrm{f}} - M_{\mathrm{p}} \tag{4}$$

Besides, the external torque consumption is mainly counted on the propeller connected to the engine. Despite of the shaft system and the gear-box also result in partial torque loss, the value is considerable small and its variation is quite slow compared with the torque generated by the propeller, so this part of torque loss is ignored in this paper. The reduction ratio of the gear-box is assumed to be 1, which is clear for analysis and will not affect the structure of the mathematical model. Hence, the external torque consumption M_{load} is equal to the propeller torque loss, and can be obtained as

$$M_{\mathrm{load}} = k n_{\mathrm{e}}^2 \tag{5}$$

where the coefficient k is calculated by $k = K_{\mathrm{M}} \rho_{\mathrm{w}} D_{\mathrm{p}}^5$ with K_{M} denoting the propeller torque coefficient, D_{p} denoting the propeller diameter, and ρ_{w} denoting the seawater density [37].

B. DIESEL ENGINE SPEED CONTROL PROBLEM FORMULATION

The dynamic model of the propulsion system can be obtained

$$\left(J_{\mathrm{e}} + J_{\mathrm{p}}\right) \frac{\mathrm{d}n_{\mathrm{e}}}{\mathrm{d}t} = \frac{30}{\pi} \left(M_{\mathrm{e}} - M_{\mathrm{load}} - M_{\mathrm{d}}\right) \tag{6}$$

where J_{e} denotes the total inertia moment of the moving components of the diesel engine, J_{p} is inertia moment of the propeller. The external disturbance M_{d} is mainly caused by the change of propeller torque, which results from the fluctuation of propeller torque coefficient and partial propeller emerging from water.

Remark 1: J_{p} is usually different for various propulsion systems and time-varying even for the same propulsion system because of the entrained water inertia [7].

Combining (1)-(6), the entire dynamic model can be summarized as

$$\dot{x} = f(x) + g(t)\, u + d(t) \tag{7}$$

where the engine speed is chosen to be system state variable and the fuel mass injected into each cylinder per cycle is taken as control input variable, i.e. $x = n_{\mathrm{e}}$ and $u = m_{\mathrm{f}}$. Besides, $f(x)$, $g(t)$ and $d(t)$ are given as follows

$$f(x) = -\frac{30}{\pi \left(J_{\mathrm{e}} + J_{\mathrm{p}}\right)} \left(M_{\mathrm{f}} + M_{\mathrm{load}}\right)$$

$$g(t) = \frac{15 q_{\mathrm{LHV}} N_{\mathrm{cyl}} \eta_{\mathrm{i}}}{\pi^2 N_{\mathrm{st}} \left(J_{\mathrm{e}} + J_{\mathrm{p}}\right)}$$

$$d(t) = -\frac{30}{\pi \left(J_{\mathrm{e}} + J_{\mathrm{p}}\right)} \left(M_{\mathrm{p}} + M_{\mathrm{d}}\right)$$

For the marine engine, speed setting mode is the main working module and the basic requirement at sea. The desired speed is sent to the controller by the telegraph, which switches values in the step form.

Remark 2: The coefficients N_{cyl}, N_{st} and q_{LHV} are constants for a given diesel engine. However, the gross indicated efficiency η_{i} is time-varying, which infers $g(t)$ is time-varying, and has significant impact on the speed control system. In this paper, η_{i} is supposed to be dominated by excess air coefficient α and engine speed n_{e}, thus it is calculated as [38], [39]

$$\eta_{\mathrm{i}} = \left(a_1 n_{\mathrm{e}}^2 + a_2 n_{\mathrm{e}} + a_3\right) \left(1 - a_4 \alpha^{a_5}\right) \tag{8}$$

where $a_i, i = 1, 2, \ldots, 5$ are experimental constants. The excess air coefficient is calculated by the qualities of the fuel injected and the air intake per cycle per cylinder. The air mass is obtained by the turbocharger model, the intake manifold model, the exhaust manifold model as shown in Fig. 1. The detailed illustration has been given in [40], and omitted here due to space limitation.

Remark 3: Although M_{p} can be calculated by (3), the measurements for p_{em} and p_{im} are not always available due to the high cost of pressure sensors. Thus, we assume that M_{p} is unknown and treated as part of external disturbances.

Given Remarks 1-3, the following assumption can be made.

Assumption 1: Denote $f(x) = f_0(x) + \Delta f(x)$ and $g(t) = g_0(t) + \Delta g(t)$, where $f_0(x)$ and $g_0(t)$ represent the known parts of $f(x)$ and $g(t)$, while $\Delta f(x)$ and $\Delta g(t)$ are the unknown parts.

In view of the above statement, system (7) is rewritten as

$$\dot{x} = f_0(x) + g_0(t)u + D \tag{9}$$

where $D = d(t) + \Delta f(x) + \Delta g(t)u$ represents the synchronized uncertainties.

Remark 4: The actuators of the speed control system are subject to input constraints and the fuel mass injected into each cylinder per cycle should be neither negative nor exceed the maximum limit of the diesel engine. Excessive fuel injection mass will shorten the service life of the diesel engine and even cause serious damage. Besides, the fuel injection mass is usually limited to ensure appropriate excess air coefficient in order to achieve economical efficiency and satisfy strict emission requirements [41].

According to Remark 4, one can get

$$u \in [0, \bar{u}] \tag{10}$$

where the positive variable $\bar{u}$ denotes the maximum limitation of fuel mass per cylinder per cycle in accordance with the working condition of the concerned diesel engine.

C. CONTROL OBJECTIVES

For marine diesel engine, steady sailing speed tracking is a key evaluation indicator. The desired speed of the marine engine is given by the telegraph, which consists of a set of fixed target speed values. The output signals of the telegraph switches between the adjacent values during the whole operation progress. Additionally, a slope limit is commonly applied on the target speed to avoid excessive acceleration for preventing propulsion system damage [37]. In practice, the marine diesel engine speed control strategy is designed to drive the engine speed to track the desired speed with fast response capability and high robustness. Meanwhile, the input constraints mentioned in Remark 4 should be taken into consideration to obtain reasonable control command, such that satisfying performance can be achieved.

D. USEFUL DEFINITIONS AND LEMMAS

Before proceeding further, several useful definitions and lemmas are introduced.

Definition 1 [42]: Consider the following system

$$\dot{x} = f(x, u), x(t_0) = x_0, \quad x \in \Re^n \tag{11}$$

where $f : D \to \Re^n$ is non-Lipschitz continuous on a neighborhood D of the origin $x = 0$ in $\Re^n$. The state variable x is finite-time convergent if there is an open neighborhood U of the origin and a function $T_x : U\setminus\{0\} \to (0, \infty)$, such that every solution trajectory $x(t, x_0)$ of (11) starting from the initial point $x_0 \in U\setminus\{0\}$ is well-defined and unique in forward time for $t \in [0, T_x(x_0))$, and $\lim_{t\to T_x(x_0)}(t, x_0) = 0$. Here $T_x(x_0)$ is called the settling time (of the initial state x_0). The state variable x of (11) is finite-time stable if it is Lyapunov stable and finite-time convergent. If $U = D = \Re^n$, the state variable x of (11) is globally finite-time stable.

Definition 2 [43]: The solution of the nonlinear system (11) is practical finite-time stable (PFS) if for all $x(t_0) = x_0$, there exist $\varepsilon > 0$ and $T(\varepsilon, x_0) < \infty$ such that $\|x(t)\| < \varepsilon$ for all $t \geq t_0 + T$.

Lemma 1 [44]: Consider system (11), and suppose that there exists continuous function $V(x)$, scalars $c > 0$ and $0 < \alpha < 1$, such that

$$\dot{V}(x) + cV(x)^{\alpha} \leq 0$$

Then the origin is finite-time stable equilibrium of the system (11). Moreover, the settling time $T_x(x_0)$ satisfies $T_x(x_0) \leq \frac{1}{c(1-\alpha)}V(x_0)^{1-\alpha}$.

Lemma 2 [43]: Considering system (11), and suppose that there exist continuous function $V(x)$, scalars $\lambda > 0, 0 < \alpha < 1$ and $0 < \beta < \infty$, such that

$$\dot{V}(x) \leq -\lambda V(x)^{\alpha} + \beta$$

Then, the trajectory of system (11) is PFS. Therefore, the trajectories of the closed-loop system are bounded in finite time as $\lim_{\theta\to\theta_0} x \in \left(V(x)^{\alpha} \leq \frac{\beta}{\lambda(1-\theta)}\right)$, where $0 < \theta_0 < 1$. And the time needed to reach such a neighborhood is bounded as $T_x(x_0) \leq \frac{V(x_0)^{1-\alpha}}{\lambda\theta_0(1-\alpha)}$, where $V(x_0)$ is the initial value of $V(x)$.

Lemma 3 [42]: For all $x_i \in \Re\ (i = 1, 2, \ldots, n)$ and real number $p \in (0, 1]$, following inequalities hold

$$\left(\sum_{i=1}^{n}|x_i|\right)^{p} \leq \sum_{i=1}^{n}|x_i|^{p} \leq n^{1-p}\left(\sum_{i=1}^{n}|x_i|\right)^{p}$$

III. FINITE-TIME OBSERVER BASED SPEED CONTROL LAW WITH INPUT CONSTRAINTS

In this section, a finite-time disturbance observer is first designed to estimate the synchronized uncertainties. Then, based on the observation information, a finite-time control law with consideration of input constraints is constructed.

A. FINITE-TIME DISTURBANCE OBSERVER

For estimating and compensating the synchronized uncertainties, a finite-time disturbance observer is developed. Define $z_1 = x$ and an extended state variable $z_2 = D$.

Assumption 2: For diesel engine speed control system, the disturbance D is continuous and differentiable. Denoting $\dot{D} = h(t)$, and $h(t)$ is assumed to be unknown but bounded, i.e. $|h(t)| < \bar{h}$ with $\bar{h}$ being a positive scalar.

Then, system (9) is extended as

$$\begin{cases} \dot{z}_1 = f_0(x) + g_0(t)u + z_2 \\ \dot{z}_2 = h(t) \end{cases} \tag{12}$$

Let $\widehat{z}_1$ and $\widehat{z}_2$ represent the estimated values for z_1 and z_2, respectively. A disturbance observer is given as follows

$$\begin{cases} \dot{\widehat{z}}_1 = f_0(x) + g_0(x)u + \widehat{z}_2 - \theta\rho_1 \mathrm{sig}^{1/2}\left(\widehat{z}_1 - z_1\right) \\ \dot{\widehat{z}}_2 = -\theta^2\rho_2 \mathrm{sgn}\left(\widehat{z}_1 - z_1\right) \end{cases} \tag{13}$$

where ρ_1, ρ_2 and θ are positive observer gains to be selected. For a given vector $x = [x_1, \ldots, x_n]^{\mathrm{T}}$ and $\gamma \in \Re$, the function $sig^{\gamma}(x) = \left[|x_1|^{\gamma}\,\mathrm{sgn}(x_1), \ldots, |x_n|^{\gamma}\,\mathrm{sgn}(x_n)\right]^{\mathrm{T}}$ is defined.

Denote the observation errors $e_j = \widehat{z}_j - z_j$, $j = 1, 2$. According to equations (12) and (13), the observation error system can be written as

$$\begin{cases} \dot{e}_1 = e_2 - \theta\rho_1 \mathrm{sig}^{1/2}(e_1) \\ \dot{e}_2 = -\theta^2\rho_2 \mathrm{sgn}(e_1) - h(t) \end{cases} \tag{14}$$

Theorem 1: Consider the system (9) under Assumptions 1-2. If the disturbance observer (13) is applied. Then, the observation errors are finite-time stable, and the settling time is bounded by $T_{obs} \le \frac{2}{c_3} V_e(\vartheta_0)^{1/2}$.

Proof: Consider the following coordinate transformation

$$\varepsilon_i = \frac{e_i}{\theta^{i-1+\bar{\theta}}}, \quad i = 1, 2$$

where $\bar{\theta} \in (0, 1)$, thus the observation error system (14) leads to

$$\begin{cases} \dot{\varepsilon}_1 = -\theta^{1-\bar{\theta}/2}\rho_1 \mathrm{sig}^{1/2}(\varepsilon_1) + \theta\varepsilon_2 \\ \dot{\varepsilon}_2 = -\theta^{1-\bar{\theta}}\rho_2 \mathrm{sgn}(\varepsilon_1) - \theta^{-(1+\bar{\theta})} h(t) \end{cases} \tag{15}$$

By defining an auxiliary variable $\boldsymbol{\vartheta} = \left[\mathrm{sig}^{1/2}(\varepsilon_1)\ \varepsilon_2\right]^{\mathrm{T}}$, a Lyapunov function candidate is constructed

$$V_e = \boldsymbol{\vartheta}^{\mathrm{T}} P \boldsymbol{\vartheta} \tag{16}$$

where $\boldsymbol{P}$ is a positive definite symmetric matrix.

In the following context, stability analysis of the error dynamic system is addressed as follows.

Step 1: A subsystem of the error dynamics (15) is considered

$$\begin{cases} \dot{\varepsilon}_1 = -\theta^{1-\bar{\theta}/2}\rho_1 \mathrm{sig}^{1/2}(\varepsilon_1) + \theta\varepsilon_2 \\ \dot{\varepsilon}_2 = -\theta^{1-\bar{\theta}}\rho_2 \mathrm{sgn}(\varepsilon_1) \end{cases} \tag{17}$$

Differentiating $\boldsymbol{\vartheta}$ along (17), it yields

$$\begin{aligned} \dot{\boldsymbol{\vartheta}} &= \begin{bmatrix} \frac{1}{2}|\varepsilon_1|^{-1/2}\left[-\theta^{1-\bar{\theta}/2}\rho_1 \mathrm{sig}^{1/2}(\varepsilon_1) + \theta\varepsilon_2\right] \\ -\theta^{1-\bar{\theta}}\rho_2 sgn(\varepsilon_1) \end{bmatrix} \\ &= |\varepsilon_1|^{-1/2} \boldsymbol{A}_{\vartheta} \boldsymbol{\vartheta} \end{aligned} \tag{18}$$

where $\boldsymbol{A}_{\vartheta} = \begin{bmatrix} -\theta^{1-\bar{\theta}/2}\rho_1 \big/ 2 & \theta/2 \\ -\theta^{1-\bar{\theta}}\rho_2 & 0 \end{bmatrix}$

From (18), the first time derivative of V_e along the subsystem (17) is obtained

$$\dot{V}_e = -|\varepsilon_1|^{-1/2} \boldsymbol{\vartheta}^{\mathrm{T}} \left(\boldsymbol{A}_{\vartheta}^{\mathrm{T}} \boldsymbol{P} + \boldsymbol{P}\boldsymbol{A}_{\vartheta}\right) \boldsymbol{\vartheta} = -|\varepsilon_1|^{-1/2} \boldsymbol{\vartheta}^{\mathrm{T}} \boldsymbol{Q} \boldsymbol{\vartheta} \tag{19}$$

where $\boldsymbol{A}_{\vartheta}^{\mathrm{T}}\boldsymbol{P} + \boldsymbol{P}\boldsymbol{A}_{\vartheta} = -\boldsymbol{Q}$. Obviously, A_{ϑ} is Hurwitz if and only if $\theta^{1-\bar{\theta}/2}\rho_1 > 0$ and $\theta^{1-\bar{\theta}}\rho_2 > 0$. Hence, there always exists a unique solution $\boldsymbol{P} > 0$ for any $\boldsymbol{Q} > 0$.

In view of the definition of V_e, it can be deduced that $|\varepsilon_1|^{1/2} \le \|\boldsymbol{\vartheta}\| \le \lambda_{\min}^{-1/2}(\boldsymbol{P}) V_e^{1/2}$. Therefore, it further has

$$\dot{V}_e \le -\lambda_{\min}^{-1/2}(\boldsymbol{P}) V_e^{1/2} \frac{\lambda_{\min}(\boldsymbol{Q})}{\lambda_{\max}(\boldsymbol{P})} V_e = -c_1 V_e^{1/2} \tag{20}$$

where $c_1 = \lambda_{\min}^{-1/2}(\boldsymbol{P}) \frac{\lambda_{\min}(\boldsymbol{Q})}{\lambda_{\max}(\boldsymbol{P})}$

Step 2: The original error dynamic system (15) will be analyzed. Taking the time derivative of V_e along (15), it has

$$\dot{V}_e \le 2\boldsymbol{\vartheta}^{\mathrm{T}}\boldsymbol{P}\begin{bmatrix} 0 \\ -h(t)\theta^{-(1+\bar{\theta})} \end{bmatrix} - c_1 V_e^{1/2} \le -(c_1 - c_2) V_e^{1/2} \tag{21}$$

where $c_2 = \frac{2\lambda_{\max}(\boldsymbol{P})\bar{h}}{\lambda_{\min}(\boldsymbol{P})\theta^{1+\bar{\theta}}}$. If θ is sufficiently large to ensure $\theta^{1+\bar{\theta}} > \frac{2\lambda_{\max}^2(\boldsymbol{P})\bar{h}}{\lambda_{\min}(\boldsymbol{Q})\sqrt{\lambda_{\min}(\boldsymbol{P})}}$, then it can be deduced that $\dot{V}_e \le -c_3 V_e^{1/2}$ with $c_3 = c_1 - c_2 > 0$. According to Lemma 1, the observation errors converge to the equilibrium in finite time with the settling time satisfying $T_{obs} \le \frac{2}{c_3} V_e(\boldsymbol{\vartheta}_0)^{1/2}$, where $\boldsymbol{\vartheta}_0$ denotes the value of $\boldsymbol{\vartheta}$ at initial time. Thus it implies that n_e and D can be estimated by $\widehat{z}_1$ and $\widehat{z}_2$ in finite time.

B. FINITE-TIME CONTROLLER WITH INPUT CONSTRAINTS

On basis of the proposed finite-time disturbance observer, the speed control scheme will be further studied. Recalling input constraints $u \in [0, \bar{u}]$ for the injected fuel mass, the following equation is introduced

$$u = v - \Delta u \tag{22}$$

where v represents the output signal of the control algorithm, u is the actual control input acting on the diesel engine, and Δu is defined as

$$\Delta u = \begin{cases} v - \bar{u}, & \bar{u} < v \\ 0, & 0 \le v \le \bar{u} \\ v, & v < 0 \end{cases} \tag{23}$$

With the assistance of (22), it is possible to compensate the extra part of the control signal, and thus facilitate the controller design and stability analysis.

Remark 5: The input difference Δu between the desired control signal v and the actual control input u cannot be too large, otherwise it will make the actuator cannot stabilize the system in real application. Similar explanation can be found in [45], [46].

The speed tracking error is defined as

$$s = x - x_{\mathrm{d}} \tag{24}$$

where x_{d} denotes the reference engine speed.

Furthermore, to facilitate controller design, an auxiliary variable is defined

$$\eta = s - \xi \tag{25}$$

Here, ξ is defined in the form of command filter

$$\dot{\xi} = -h_1\xi - h_2\xi^r - g_0(t)\,\Delta u \tag{26}$$

with h_1, h_2 being positive gains and $0 < r < 1$.

Thus, the finite-time speed control law with input constraints is proposed

$$v = g_0(t)^{-1}\left[-h_1 s - h_2\xi^r - h_3\eta^r - f_0(x) - \widehat{z}_2 + \dot{x}_{\mathrm{d}}\right] \tag{27}$$

where h_1 and h_2 are positive control gains to be chosen.

Theorem 2: Consider system (9) under Assumptions 1-2. If controller (27) combined with observer (13) is applied. Then, the system trajectories are practical finite-time stable.

Proof: A Lyapunov candidate function is selected as

$$V = V_1 + V_2 \tag{28}$$

where $V_1 = \frac{1}{2}\eta^{\mathrm{T}}\eta$ and $V_2 = \frac{1}{2}\xi^{\mathrm{T}}\xi$.

Combining (24), (25) and (26), the time derivative of η yields

$$\begin{aligned}\dot{\eta} &= \dot{s} - \dot{\xi}\\ &= f_0(x) + g_0(t)\,u + D - \dot{x}_{\mathrm{d}} - \left[-h_1\xi - h_2\xi^r - g_0(t)\,\Delta u\right]\\ &= f_0(x) + g_0(t)\,v + D + h_1\xi + h_2\xi^r - \dot{x}_{\mathrm{d}}\end{aligned} \tag{29}$$

Substituting control law (27) into (29), it has

$$\begin{aligned}\dot{\eta} &= -h_1 s - h_2\xi^r - h_3\eta^r - \widehat{z}_2 + \dot{x}_{\mathrm{d}} + D + h_1\xi + h_2\xi^r - \dot{x}_{\mathrm{d}}\\ &= -h_1\eta - h_3\eta^r - e_2\end{aligned} \tag{30}$$

It has been proven in Theorem 1 that the observation error e_2 approaches zero within finite time. Hence, stability of the closed-loop system is analyzed by two phases.

Firstly, before the settling time T_{obs}, the time-derivative of (28) yields

$$\begin{aligned}\dot{V} &= -h_1\eta^{\mathrm{T}}\eta - h_3\eta^{r+1} - \eta^{\mathrm{T}}e_2 - h_1\xi^{\mathrm{T}}\xi - h_2\xi^{r+1}\\ &\quad -\xi^{\mathrm{T}}g_0(t)\,\Delta u\\ &\le -\left(h_1 - \frac{1}{2}\right)\eta^{\mathrm{T}}\eta - h_3\eta^{r+1} - \left(h_1 - \frac{1}{2}\right)\xi^{\mathrm{T}}\xi - h_2\xi^{r+1}\\ &\quad +\frac{1}{2}\|e_2\|^2 + \frac{1}{2}\|g_0(t)\,\Delta u\|^2\end{aligned} \tag{31}$$

Since the observation error e_2 converges to zero in finite time, it can be concluded that $\|e_2\| \le \rho_1$ with ρ_1 being a positive scalar. Moreover, it is reasonable to assume that $\|g_0(t)\,\Delta u\| \le \rho_2$ with ρ_2 being a positive scalar, for $g_0(t)$ is a constant calculated by the engine coefficient and Δu should be a bounded constant with consideration of Remark 5.

Hence, (31) leads to

$$\begin{aligned}\dot{V} &\le -\left(h_1 - \frac{1}{2}\right)\eta^{\mathrm{T}}\eta - \left(h_1 - \frac{1}{2}\right)\xi^{\mathrm{T}}\xi + \frac{1}{2}\rho_1^2 + \frac{1}{2}\rho_2^2\\ &\le -\rho_3 V + \rho_4\end{aligned} \tag{32}$$

where $\rho_3 = 2h_1 - 1$ and $\rho_4 = \frac{1}{2}\rho_1^2 + \frac{1}{2}\rho_2^2$. Thus, it further implies that the closed-loop system is ultimately bounded stable and the states η and ξ converge to a region around the equilibrium if any of the following inequalities satisfied

$$\eta \ge 2\rho_4/\rho_3$$

$$\xi \ge 2\rho_4/\rho_3$$

Therefore, it can be concluded that the system states η and ξ are bounded even before the synchronized uncertainties are precisely compensated.

Secondly, after the settling time T_{obs}, the observation error $e_2 = 0$, then (30) can be simplified as

$$\dot{\eta} = -h_1\eta - h_3\eta^r \tag{33}$$

Given (26) and (33), then differentiating the Lyapunov function V, it yields

$$\dot{V} = -h_1\eta^{\mathrm{T}}\eta - h_3\eta^{r+1} - h_1\xi^{\mathrm{T}}\xi - h_2\xi^{r+1} - \xi^{\mathrm{T}}g_0(t)\,\Delta u \tag{34}$$

By using Young's inequality, it can be obtained

$$\begin{aligned}\dot{V} &\le -h_1\eta^{\mathrm{T}}\eta - h_3\eta^{r+1} - \left(h_1 - \frac{1}{2}\right)\xi^{\mathrm{T}}\xi - h_2\xi^{r+1}\\ &\quad +\frac{1}{2}\|g_0(t)\,\Delta u\|^2\\ &\le -(2h_1 - 1)\,V - 2^{\frac{r+1}{2}}\lambda\left(V_1^{\frac{r+1}{2}} + V_2^{\frac{r+1}{2}}\right)\\ &\quad +\frac{1}{2}\|g_0(t)\,\Delta u\|^2\end{aligned} \tag{35}$$

where $h_1 > \frac{1}{2}$ and $\lambda = \min\{h_2, h_3\} > 0$.

In view of Lemma 3, one can get $V^{\frac{r+1}{2}} = (V_1 + V_2)^{\frac{r+1}{2}} \le V_1^{\frac{r+1}{2}} + V_2^{\frac{r+1}{2}}$, then (35) leads to

$$\dot{V} \le -2^{\frac{r+1}{2}}\lambda V^{\frac{r+1}{2}} + \frac{1}{2}\|g_0(t)\,\Delta u\|^2 \tag{36}$$

According to Lemma 2, the system (9) with the control law (27) is practical finite-time stable. For all $x(t_0) = x_0$, the time in which the system trajectory reach

$$\lim_{\omega\to\omega_0} x \in \left(V^{\frac{r+1}{2}} \le \|g(t)\,\Delta u\|^2 \Big/ 2^{\frac{3+r}{2}}\lambda(1-\omega)\right)$$

And the settling time satisfies $T \le (2V(x_0))^{\frac{1-r}{2}} \Big/ \lambda\omega_0(1-r)$, where $0 < \omega_0 < 1$, $V(x_0)$ is the initial value of $V(x)$.

Therefore, η and ξ are proven to be PFS. Actually, control signal v decreases as the speed tracking error approaching the equilibrium. Eventually, v will fluctuate between the upper bound and lower bound, thus the final value of Δu is zero. Hence, ξ is finite-time stable from (26). Given (25), it can be deduced that speed tracking error s is practical finite time stable.

Remark 6: Compared with the control methods in [5]–[13], it is noticeable that not only finite-time convergence rate is achieved but also the input constraints problem is explicitly handled in this paper. Given the fact that the fuel injectors only respond to the positive control signals, the proposed speed control law with input constraints possesses practical significance and application value.

Remark 7: The proposed control scheme is developed on basis of the MVEM, which is a common model for diesel engine and gasoline direct injection engine. Therefore, this

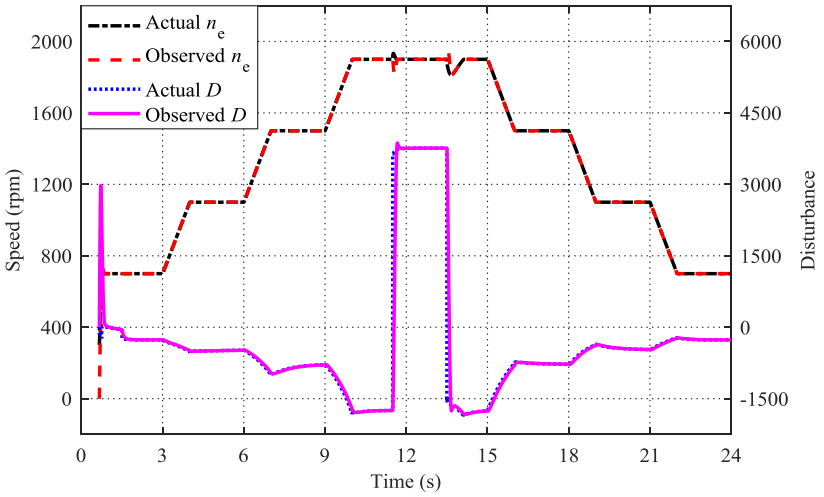

FIGURE 2. The overall tracking performance of the disturbance observer.

TABLE 1. Parameters of the marine diesel engine.

Parameter	Value
Working Principle	4-stroke
No. of Cylinders	In-line, 6
Bore/Stroke	130/160 mm
Displacement	12.7L
Compression Ratio	17.5:1
Intake System	Turbocharging, inter-cooling
Rated Power	405kW (1900rpm)
Maximum Fuel Delivery	250mg/cycle

method can be easily extended to the case of gasoline direct injection engines. However, for the non-gasoline direct injection engines, further research should be carried out in the near future, because the throttle motion model has not been considered by now.

IV. SIMULATION AND ANALYSIS

To verify the effectiveness of the proposed finite-time observer based control law (FTOBC), numerical simulation on a marine diesel engine is carried out, the results are analyzed in this section. Moreover, the second order sliding mode controller (SOSMC) in [13] is employed under the same simulated condition, which has shown better performance than traditional PID controller. Hence, by comparing the results between SOSMC and FTOBC, the superiority of FTOBC is illustrated.

In Table 1, the primary parameters of the concerned marine diesel engine are given. According to the common operating conditions of marine diesel engines, the simulations include the starting process, steady operation process, acceleration and deceleration between speed set points, and sudden load changing. To get the engine running, a starting torque is used to drive the engine until it reaches a certain speed, then the control algorithms will take charge of the speed control system. A set of reference speed is considered as set points to test control performance, which are 700 rpm, 1100 rpm, 1500 rpm and 1900 rpm. After the starting process, the reference speed changes between the adjacent set points. A slope limit is applied on the reference speed, which is set as 400 rpm/s. Besides, in harsh sea conditions, the propeller inevitably emerges and reenters the water, which would cause dramatic loads changing. Given such situation, propeller torque M_{load} is discharged and increased by 50% at 11.5 s and 12.5 s to simulate the effect of emerging and reentering. Especially, varied inertia moment J_p and diverse slope limits are considered to test the robustness of the proposed FTOBC.

A. DISTURBANCE OBSERVER PERFORMANCE

The simulation results of the finite-time disturbance observer (13) are given in Fig. 2-4, where the parameters are chosen as $\theta = 10$, $\rho_1 = 20$ and $\rho_2 = 30.5$.

Due to the starting process, the disturbance observer is initiated at about 0.66s when the FTOBC takes over the control authority. From Fig. 2, it can be seen that the synchronized uncertainties D varies with the changing of engine speed n_e and propeller torque. Meanwhile, the response curves of the observation value keep good tracking performance during the whole working process. More details are depicted in Fig. 3 and Fig. 4.

Fig. 3 (a) and (d) show the trajectories of engine speed n_e, synchronized uncertainties D, and their observations after the algorithm execution. It only takes the finite-time observer less than 0.2 s to stabilize the observation errors with considerable high accuracy. In Figs. 3 (b) and (c), the observed results of engine speed during acceleration and deceleration processes are presented, which indicate that the observed n_e can track the time-varying actual speed with negligible overshoot and acceptable accuracy. Correspondingly, Fig. 3 (e) and (f) show

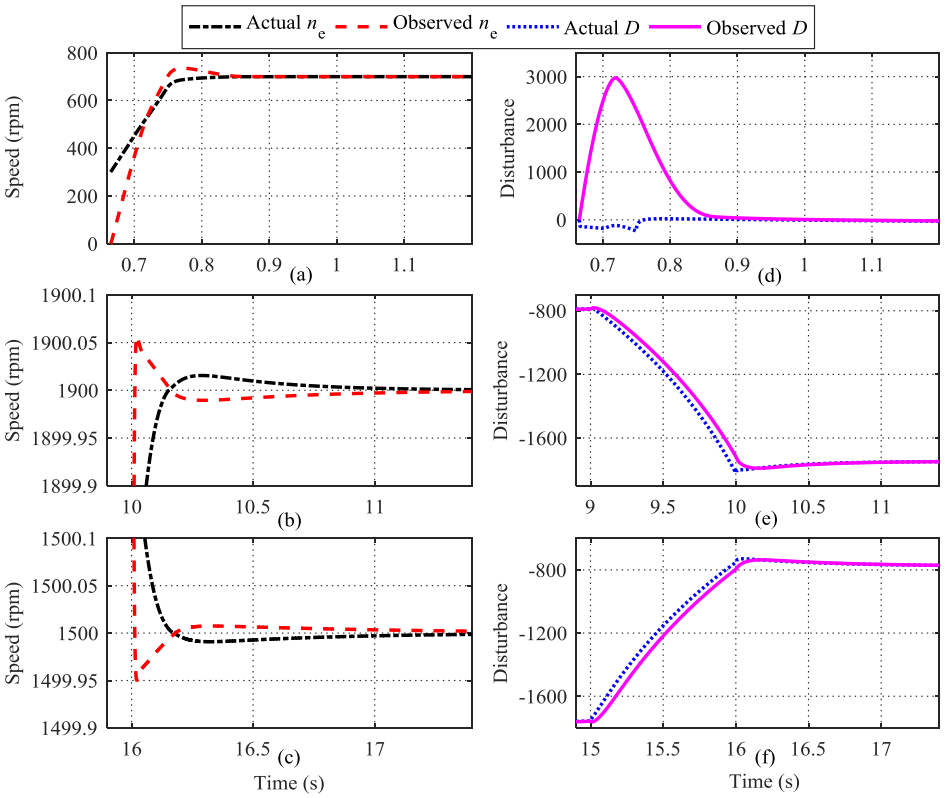

FIGURE 3. The detail tracking performance of the disturbance observer during (a) and (d) starting, (b) and (e) acceleration from 1500 rpm to 1900 rpm, (c) and (f) deceleration from 1500 rpm to 1900 rpm.

that there is a slight delay deviation of the observed D during acceleration and deceleration process, and the observation can track its real value precisely afterwards.

The abrupt loading and unloading are big challenges for marine diesel engine control system, thus Fig. 4 is carried out. The propeller torque M_{load} is discharged and increased by 50% at 11.5 s and 12.5 s, respectively. Due to the sudden reversed change of $g_0(t) \cdot u$, the time history of observed speed diverges from the actual speed at the beginning. Then, it consumes approximate 0.2 s for the observation errors to be stabilized. Hence, it can be seen that the observed speed and observed disturbance track their actual value despite the instant change of load.

To sum up, the proposed finite-time disturbance observer possesses good tracking performance and considerable fast convergence rate, which can be used for control law implement.

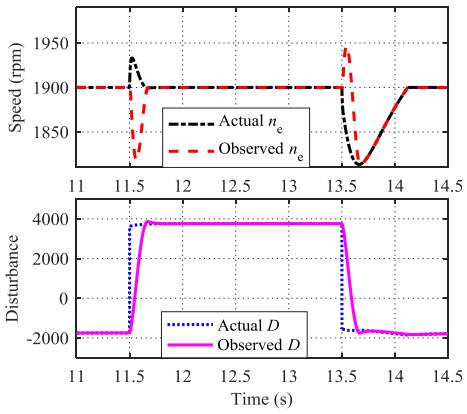

FIGURE 4. The detail tracking performance of the disturbance observer during loading and unloading.

B. FINITE-TIME CONTROLLER PERFORMANCE

In order to illustrate the advantages of FTOBC, a SOSMC controller proposed in [13] is applied on the concerned marine diesel engine for comparison. Moreover, the parameters of both controllers are selected by balancing the control performance under different working conditions. The control parameters of the FTOBC are selected as $r = 0.8$, $h_1 = 92$, $h_2 = 110$ and $h_3 = 98$. The parameters of SOSMC are chosen as $\rho = 0.5$, $\lambda_1 = 5.5$ and $\lambda_2 = 80$.

Additionally, the input constraints for the two controllers are considered in two aspects: the upper and lower bounds. The upper bound, i.e. the limit of SOSMC/FTOBC in the following figures, refers to the maximum allowed value of fuel mass per cylinder per cycle. To be specific, it is calculated in real time with consideration of the minimum limit value of excess air coefficient and the air intake mass. Meanwhile, it should be bounded by the maximum allowed fuel mass by the concerned engine, i.e. 250mg/cycle. Since the air intake mass varies with the engine operating conditions,

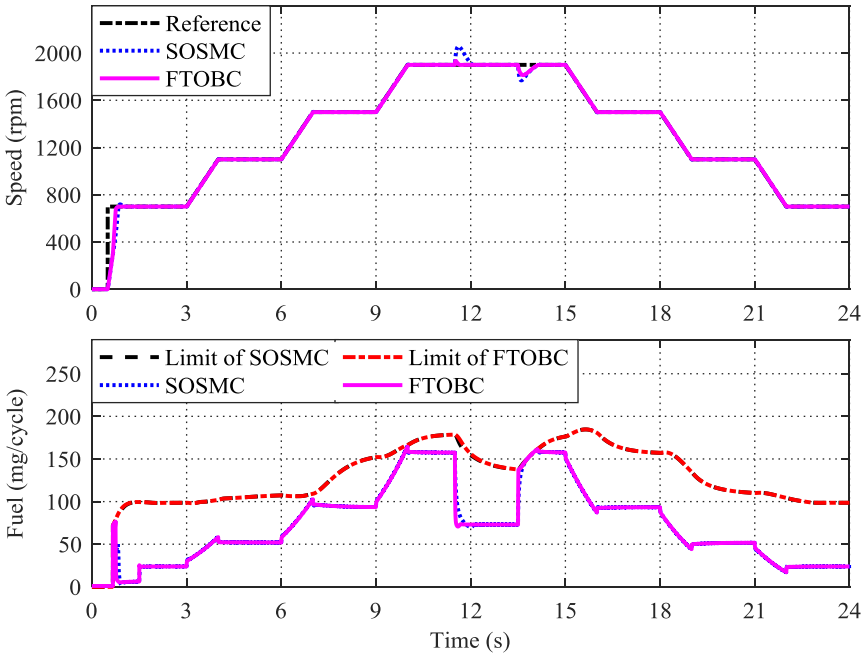

FIGURE 5. The control performance comparison between SOSMC and FTOBC.

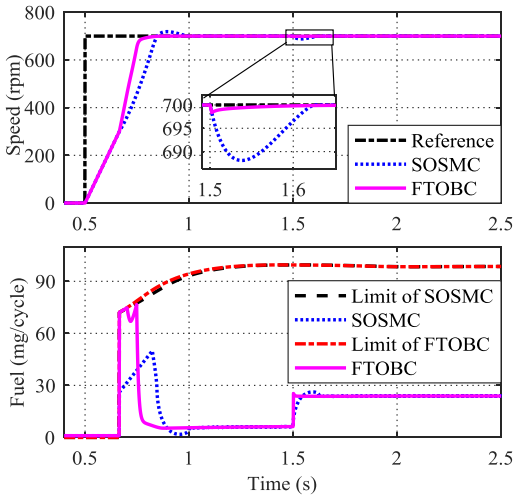

FIGURE 6. The starting process comparison between SOSMC and FTOBC.

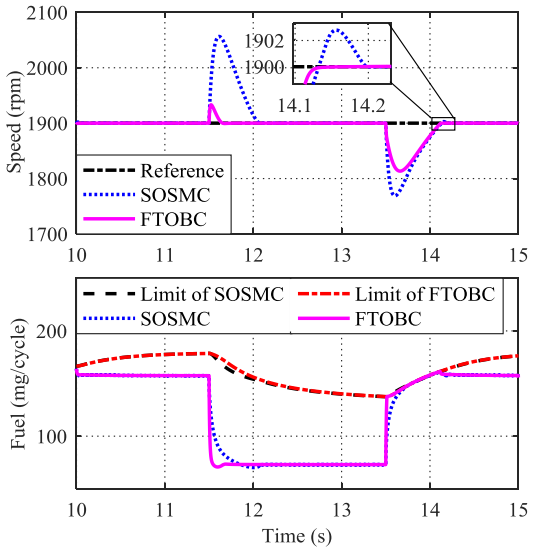

FIGURE 7. Diesel engine speed and controller output response during loading and unloading.

the maximum allowed value of fuel mass is also time-varying as shown in Fig. 5. The lower bound for both controllers is set as zero, for only positive fuel amount is possible to be injected. Although SOSMC is designed regardless of control input constraints, the above mentioned upper/lower bound should be applied to SOSMC in the simulation, thus fair comparison of control performance can be ensured.

The results of engine speed and control output response curves under FTOBC and SOSMC are shown in Fig. 5-9. From Fig. 5, we can see that both controllers process satisfying performance under each operating condition. Detailed description and analysis are described below.

1) CASE 1 STARTING PROCESS

Simulation results for the starting process are presented in Fig. 6. The control algorithms effect on the engine instead of the starting torque as the speed reaching 300 rpm, which would lead to speed fluctuation to some extent. The overshoot of the engine speed under the FTOBC is attenuated and the recovery time is less than 0.33 s. Whereas, the overshoot and recovery time are 21.8 rpm and 0.49 s when SOSMC is applied. After the speed is stabilized at idle value, the torque generated by the propeller is loaded on the engine at 1.5 s,

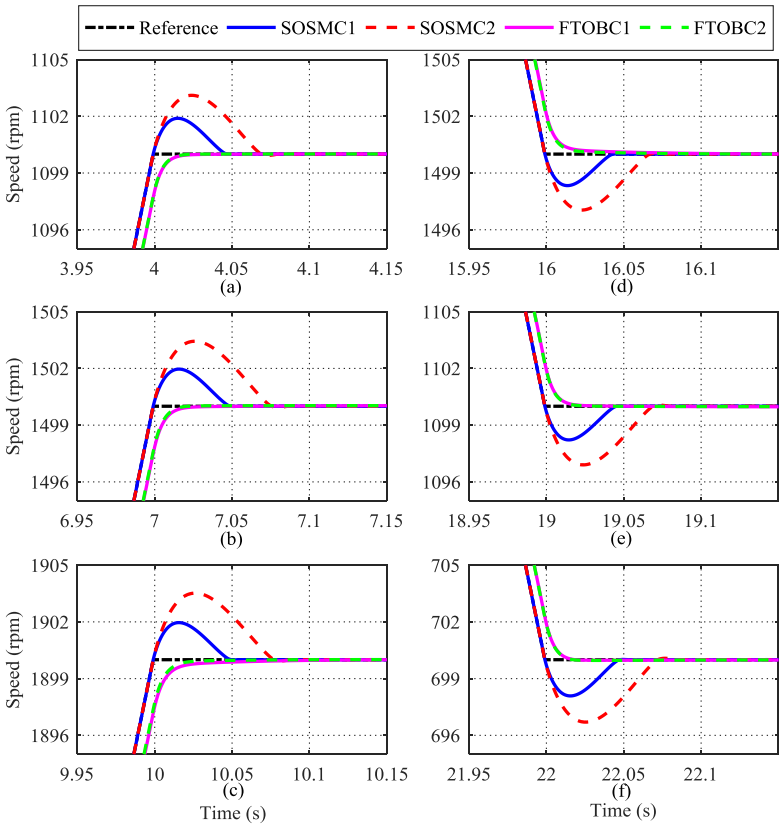

FIGURE 8. The control performance comparison between SOSMC and FTOBC with different moment of inertia under various conditions like (a) acceleration from 700 rpm to 1100 rpm, (b) acceleration from 1100 rpm to 1500 rpm, (c) acceleration from 1500 rpm to 1900 rpm, (d) deceleration from 1900 rpm to 1500 rpm, (e) deceleration from 1500 rpm to 1100 rpm and (f) deceleration from 1100 rpm to 700 rpm.

which results in an overshoot of approximate 12 rpm and 0.12 s recovery time for SOSMC. However, it only brings a 2 rpm overshoot for FTOBC, and the recovery time is 0.08 s. As shown in Fig. 6, by applying FTOBC scheme, the fuel mass reaches the upper bound for a while at the beginning stage, then drops sharply and stays within the allowed range. Owing to the large magnitude of control output, FTOBC possesses faster response speed than SOSMC. Moreover, the fuel mass immediately falls back into the allowed range after reaching the upper bound, because the input constraints problem has been handled by algorithm design. Hence, by considering input constraints, control performance of FTOBC is improved.

2) CASE 2 LOADING AND UNLOADING CONDITIONS

As stated previously, dramatic load changing would happen when the propeller emerges from the water and renters into water. Fig. 7 shows the simulation result when 50% load is suddenly unloading and loading at 1900 rpm. It can be observed that control performance of FTOBC is obviously superior to SOSMC. During the unloading phase, the overshoot under FTOBC is only 34 rpm, which is obviously less than the overshoot of 156 rpm under SOSMC. Meanwhile, the recovery time of FTOBC and SOSMC turns out to be 0.14 s and 0.56 s, respectively. During the loading phase, because of the delay of turbocharge, the fuel mass under both controllers have once reached their limits. Therefore, the engine speed overshoot under the both controllers are larger, i.e. 87 rpm and 132 rpm for the FTOBC and SOSMC, respectively. Besides, because of the integral item in the SOSMC controller, the control signal still increases even when the limit is reached. Hence, an overcontrolling is caused, which is shown by the enlarged plot. This phenomenon is likely to occur in the presence of integral loops and can be weakened by setting limitation in integral item or with anti-windup methods [47], [48], but such methods can hardly keep good performance during the wide operating conditions for diesel engine. Nevertheless, FTOBC avoids this situation and recovered faster.

3) CASE 3 ACCELERATION AND DECELERATION CONDITIONS WITH DIFFERENT INERTIA MOMENT

In practical, a diesel engine is required to be able to work with different propulsion system rather than a fixed one. Hence, varied system parameters for distinct propulsion should be taken into consideration, such as inertia moment, torque

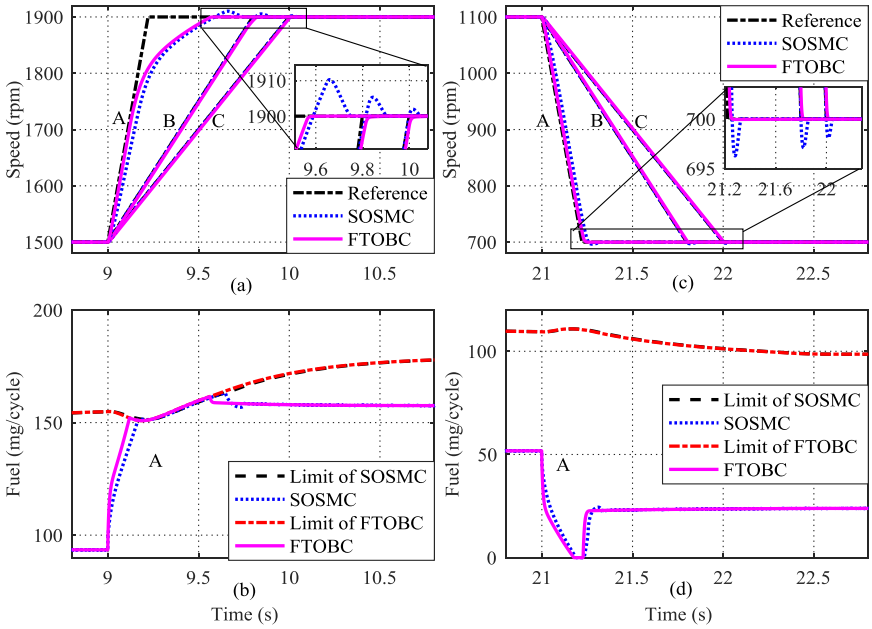

FIGURE 9. Robust comparison of the two controllers with different desired speed slope limits, A-2000 rpm/s, B-500 rpm/s, C-400rpm/s.

coefficient, etc. In this case, the concerned control strategies are applied on propulsion systems with different inertia moments, thus robustness of the FTOBC and SOSMC can be verify and compared. Two sets of propulsion system parameters are selected. Control gains for both FTOBC and SOSMC are tuned for only one set, thus system robustness of the two schemes is tested. Accordingly, the response curves are denoted as SOSMC1 and FTOBC1 for one set, SOSMC2 and FTOBC2 for the other set. In Fig. 8, during acceleration/deceleration stage, a slight speed delay deviation exists when FTOBC is applied, whereas accurately tracking is performed by SOSMC. That is because a small deviation exists between the observed D and the actual D at the above mentioned stage, which has been shown in Fig. 3. After the acceleration/deceleration, engine speed under the FTOBC converges to the reference speed within 0.05 s. Whereas it takes SOSMC much longer time to stabilize engine speed to the set points and obvious overshoot can be observed. Although both controllers achieve speed tracking with high accuracy after a certain time, control performance of SOSMC deteriorates as the propulsion system parameters changed. However, FTOBC scheme maintains satisfactory performance under different propulsion inertia moment, which implies that FTOBC demonstrates stronger robustness compared with SOSMC.

4) CASE 4 ACCELERATION AND DECELERATION CONDITIONS WITH DIFFERENT SLOPE LIMITS

From the perspective of safe operation, distinct propulsion systems should match different slope limits. Hence, the following processes are carried out to test control performance of FTOBC and SOSMC under varied slope limits. In Fig. 9, the black dash line A, B and C denote three types of slope limit, which are 2000 rpm/s, 500 rpm/s and 400 rpm/s respectively. Observed from Fig. 9 that FTOBC performs satisfactorily with high tracking accuracy under all three cases, whereas system performance is heavily affected by the slope limit when SOSMC applied. It is worthwhile to mention that extreme large/small injection volume is inevitable for driving engine speed to track steep slope limit. Hence, the upper and lower bound of fuel mass are reached when tracking the 2000rpm/s slope under both controllers. However, the response curves of FTOBC recover faster with less fluctuation afterwards, due to input constraints problem has been solved by the algorithm in advance.

Summarizing the above analysis and comparison, FTOBC scheme shows superior performance over SOSMC scheme. Accurate speed tracking with fast convergence rate and strong robustness are guaranteed by FTOBC, and input constraints problem is also solved properly as well. Therefore, control performance of marine diesel engine speed system can be further improved by the proposed FTOBC.

V. CONCLUSION AND PERSPECTIVES

In this paper a finite-time observer-based speed control method is investigated to handle system uncertainties, external disturbances and the inherent input constraints problem. By proposing a finite-time disturbance observer, synchronized uncertainties including parametric uncertainties and external disturbances are reconstructed. Based on the observation information, a finite-time control law with input constraints is further designed. Theoretical analysis proofs that system trajectories converge to a small neighborhood around the equilibrium within finite-time. To show the superior

performance over the existing methods, numerical simulation is carried out. By comparing the results of various operation situations on the marine diesel engine, faster convergence rate and stronger robustness are demonstrated by the proposed FTOBC while achieving precise speed tracking. Our future work will concern the discontinuity and inhomogeneity of the diesel engine, and control algorithms will be tested on real engine bench.

ACKNOWLEDGMENT

The authors would like to thank the Editor-in-Chief, Associate Editor, and anonymous referees for their invaluable comments and suggestions.

REFERENCES

[1] N. Xiros, *Robust Control of Diesel Ship Propulsion*. London, U.K.: Springer, 2002, pp. 1–3.
[2] R. D. Geertsma, R. R. Negenborn, K. Visser, and J. J. Hopman, "Design and control of hybrid power and propulsion systems for smart ships: A review of developments," *Appl. Energy*, vol. 194, pp. 30–54, May 2017.
[3] A. S. Ramadhas, C. Muraleedharan, and S. Jayaraj, "Reduction in exhaust gas temperature of biodiesel fueled engine by exhaust gas recirculation," *CLEAN Soil, Air, Water*, vol. 36, no. 12, pp. 978–983, Dec. 2008.
[4] Hu, Yang, Li, Li, and Bai, "Intelligent control strategy for transient response of a variable geometry turbocharger system based on deep reinforcement learning," *Processes*, vol. 7, no. 9, p. 601, Sep. 2019.
[5] S.-H. Lee, J.-S. Yim, J.-H. Lee, and S.-K. Sul, "Design of speed control loop of a variable speed diesel engine generator by electric governor," in *Proc. IEEE Ind. Appl. Soc. Annu. Meeting*, Oct. 2008, pp. 159–163.
[6] D. J. McGowan, D. J. Morrow, and B. Fox, "Integrated governor control for a diesel-generating set," *IEEE Trans. Energy Convers.*, vol. 21, no. 2, pp. 476–483, Jun. 2006.
[7] N. I. Xiros, "PID marine engine speed regulation under full load conditions for sensitivity H_∞-norm specifications against propeller disturbance," *J. Mar. Eng. Technol.*, vol. 3, no. 2, pp. 3–11, Jan. 2004.
[8] F. A. Mohamed and H. N. Koivo, "Diesel engine systems with genetic algorithm self tuning PID controller," in *Proc. Int. Conf. Future Power Syst.*, Nov. 2005, p. 4.
[9] R. Wang, X. Li, Y. Liu, W. Fu, S. Liu, and X. Ma, "Multiple model predictive functional control for marine diesel engine," *Math. Problems Eng.*, vol. 2018, pp. 1–20, May 2018.
[10] M. Ouladsine, G. Bloch, and X. Dovifaaz, "Neural modelling and control of a diesel engine with pollution constraints," *J. Intell. Robotic Syst.*, vol. 41, nos. 2–3, pp. 157–171, Jan. 2005.
[11] Y. Yuan, Y. He, L. Cai, and X. Mao, "Discrete sliding mode variable structure control over the rotating speed of marine diesel engines," *Proc. Inst. Mech. Eng. I, J. Syst. Control Eng.*, vol. 231, no. 5, pp. 367–379, May 2017.
[12] Y. Yuan, M. Zhang, Y. Chen, and X. Mao, "Multi-sliding surface control for the speed regulation system of ship diesel engines," *Trans. Inst. Meas. Control*, vol. 40, no. 1, pp. 22–34, Jan. 2018.
[13] X. Li, Q. Ahmed, and G. Rizzoni, "Nonlinear robust control of marine diesel engine," *J. Mar. Eng. Technol.*, vol. 16, no. 1, pp. 1–10, Jan. 2017.
[14] Q. Lan, S. Li, J. Yang, and L. Guo, "Finite-time control for soft landing on an asteroid based on line-of-sight angle," *J. Franklin Inst.*, vol. 351, no. 1, pp. 383–398, Jan. 2014.
[15] S. Khoo, L. Xie, and Z. Man, "Robust finite-time consensus tracking algorithm for multirobot systems," *IEEE/ASME Trans. Mechatronics*, vol. 14, no. 2, pp. 219–228, Apr. 2009.
[16] W. Sun, S.-F. Su, J. Xia, and Y. Wu, "Adaptive tracking control of wheeled inverted pendulums with periodic disturbances," *IEEE Trans. Cybern.*, to be published, doi: 10.1109/TCYB.2018.2884707.
[17] S. Yu and X. Long, "Finite-time consensus for second-order multi-agent systems with disturbances by integral sliding mode," *Automatica*, vol. 54, pp. 158–165, Apr. 2015.
[18] P. Liu, H. Yu, and S. Cang, "Adaptive neural network tracking control for underactuated systems with matched and mismatched disturbances," *Nonlinear Dyn.*, vol. 98, no. 2, pp. 1447–1464, Oct. 2019.
[19] Y. Liu, Y. Fu, W. He, and Q. Hui, "Modeling and observer-based vibration control of a flexible spacecraft with external disturbances," *IEEE Trans. Ind. Electron.*, vol. 66, no. 11, pp. 8648–8658, Nov. 2019.
[20] J. Zhai and H. R. Karimi, "Global output feedback control for a class of nonlinear systems with unknown homogenous growth condition," *Int. J. Robust Nonlinear Control*, vol. 29, no. 7, pp. 2082–2095, May 2019.
[21] X. Wei and L. Guo, "Composite disturbance-observer-based control and terminal sliding mode control for non-linear systems with disturbances," *Int. J. Control*, vol. 82, no. 6, pp. 1082–1098, Jun. 2009.
[22] G. Yu, H. Ogai, and H. Deng, "Offset-free model predictive control of diesel engine by combined design of disturbance model and observer," *IEEJ Trans. Electr. Electron. Eng.*, vol. 14, no. 1, pp. 116–129, Jan. 2019.
[23] J. Zhai and H. R. Karimi, "Universal adaptive control for uncertain nonlinear systems via output feedback," *Inf. Sci.*, vol. 500, pp. 140–155, Oct. 2019.
[24] B. Li, Q. Hu, and Y. Yang, "Continuous finite-time extended state observer based fault tolerant control for attitude stabilization," *Aerosp. Sci. Technol.*, vol. 84, pp. 204–213, Jan. 2019.
[25] J. Wang, S. Li, J. Yang, B. Wu, and Q. Li, "Finite-time disturbance observer based non-singular terminal sliding-mode control for pulse width modulation based DC–DC buck converters with mismatched load disturbances," *IET Power Electron.*, vol. 9, no. 9, pp. 1995–2002, Jul. 2016.
[26] N. Wang, C. Qian, J.-C. Sun, and Y.-C. Liu, "Adaptive robust finite-time trajectory tracking control of fully actuated marine surface vehicles," *IEEE Trans. Control Syst. Technol.*, vol. 24, no. 4, pp. 1454–1462, Jul. 2016.
[27] H. Chen and N. Sun, "Nonlinear control of underactuated systems subject to both actuated and unactuated state constraints with experimental verification," *IEEE Trans. Ind. Electron.*, to be published, doi: 10.1109/TIE.2019.2946541.
[28] W. Sun, S.-F. Su, Y. Wu, J. Xia, and V.-T. Nguyen, "Adaptive fuzzy control with high-order barrier Lyapunov functions for high-order uncertain nonlinear systems with full-state constraints," *IEEE Trans. Cybern.*, to be published, doi: 10.1109/TCYB.2018.2890256.
[29] W. Sun, S.-F. Su, J. Xia, and V.-T. Nguyen, "Adaptive fuzzy tracking control of flexible-joint robots with full-state constraints," *IEEE Trans. Syst., Man, Cybern., Syst.*, vol. 49, no. 11, pp. 2201–2209, Nov. 2019.
[30] N. Sun, Y. Fu, T. Yang, J. Zhang, Y. Fang, and X. Xin, "Nonlinear motion control of complicated dual rotary crane systems without velocity feedback: Design, analysis, and hardware experiments," *IEEE Trans. Autom. Sci. Eng.*, to be published, doi: 10.1109/TASE.2019.2961258.
[31] Y.-F. Gao, X.-M. Sun, C. Wen, and W. Wang, "Observer-based adaptive NN control for a class of uncertain nonlinear systems with nonsymmetric input saturation," *IEEE Trans. Neural Netw. Learn. Syst.*, vol. 28, no. 7, pp. 1520–1530, Jul. 2017.
[32] M. Chen, S.-D. Chen, and Q.-X. Wu, "Sliding mode disturbance observer-based adaptive control for uncertain MIMO nonlinear systems with dead-zone: Sliding mode disturbance observer-based adaptive control for uncertain MIMO nonlinear systems with dead-zone," *Int. J. Adapt. Control Signal Process.*, vol. 31, no. 7, pp. 1003–1018, Jul. 2017.
[33] S. Ik Han and J. Lee, "Finite-time sliding surface constrained control for a robot manipulator with an unknown deadzone and disturbance," *ISA Trans.*, vol. 65, pp. 307–318, Nov. 2016.
[34] K. V. Nielsen, M. Blanke, L. Eriksson, and M. Vejlgaard-Laursen, "Marine diesel engine control to meet emission requirements and maintain maneuverability," *Control Eng. Pract.*, vol. 76, pp. 12–21, Jul. 2018.
[35] G. Theotokatos, C. Guan, H. Chen, and I. Lazakis, "Development of an extended mean value engine model for predicting the marine two-stroke engine operation at varying settings," *Energy*, vol. 143, pp. 533–545, Jan. 2018.
[36] J. B. Heywood, *Internal Combustion Engine Fundamentals*. New York, NY, USA: McGraw-Hill, 1998, pp. 715–719.
[37] P. Mizythras, E. Boulougouris, and G. Theotokatos, "Numerical study of propulsion system performance during ship acceleration," *Ocean Eng.*, vol. 149, pp. 383–396, Feb. 2018.
[38] J. W. Chung, N. H. Kim, D. J. Kim, and S. S. Jang, "Mean value WGT diesel engine calibration model for effective simulation research," *Int. J. Automot. Technol.*, vol. 19, no. 2, pp. 209–220, Apr. 2018.
[39] L. Guzzella and A. Amstutz, "Control of diesel engines," *IEEE Control Syst.*, vol. 18, no. 5, pp. 53–71, Oct. 1998.
[40] J. Wahlström and L. Eriksson, "Modelling diesel engines with a variable-geometry turbocharger and exhaust gas recirculation by optimization of model parameters for capturing non-linear system dynamics," *Proc. Inst. Mech. Eng. D, J. Automobile Eng.*, vol. 225, no. 7, pp. 960–986, Jul. 2011.

[41] C. Gurel, E. Ozmen, M. Yilmaz, D. Aydin, and K. Koprubasi, "Multi-objective optimization of transient air-fuel ratio limitation of a diesel engine using DoE based Pareto-optimal approach," *SAE Int. J. Commercial Vehicles*, vol. 10, no. 1, pp. 299–307, 2017.
[42] G. H. Hardy, J. E. Littlewood, and G. Pólya, *Inequalities*. Cambridge, U.K.: Cambridge Univ. Press, 1952, pp. 31–32.
[43] Z. Zhu, Y. Xia, and M. Fu, "Attitude stabilization of rigid spacecraft with finite-time convergence," *Int. J. Robust Nonlinear Control*, vol. 21, no. 6, pp. 686–702, Apr. 2011.
[44] S. P. Bhat and D. S. Bernstein, "Finite-time stability of continuous autonomous systems," *SIAM J. Control Optim.*, vol. 38, no. 3, pp. 751–766, Jan. 2000.
[45] M. Chen, B. Ren, Q. Wu, and C. Jiang, "Anti-disturbance control of hypersonic flight vehicles with input saturation using disturbance observer," *Sci. China Inf. Sci.*, vol. 58, no. 7, pp. 1–12, Jul. 2015.
[46] L. Sun and Z. Zheng, "Disturbance-Observer-Based robust backstepping attitude stabilization of spacecraft under input saturation and measurement uncertainty," *IEEE Trans. Ind. Electron.*, vol. 64, no. 10, pp. 7994–8002, Oct. 2017.
[47] O. I. Borisov, V. S. Gromov, A. A. Pyrkin, A. A. Bobtsov, I. V. Petranevsky, and A. O. Klyunin, "Output robust control with anti-windup compensation for robotic boat," in *Proc. 21st Int. Conf. Methods Models Autom. Robot. (MMAR)*, Aug. 2016, pp. 13–18.
[48] C. M. R. Oliveira, M. L. Aguiar, J. R. B. A. Monteiro, W. C. A. Pereira, G. T. Paula, and T. E. P. Almeida, "Vector control of induction motor using an integral sliding mode controller with anti-windup," *J. Control, Autom. Electr. Syst.*, vol. 27, no. 2, pp. 169–178, Apr. 2016.

XUEMIN LI graduated from Southwest Jiaotong University, in 1994. He received the M.S. and Ph.D. degrees from Jilin University, in 2002 and 2005, respectively, all in internal combustion engine.

In 2005, he joined the College of Power and Energy Engineering, Harbin Engineering University, where he worked as an Assistant Professor of marine diesel control. In August 2013, he was appointed as a Professor of power mechanical and engineering with Harbin Engineering University. His main research interest is the electronic control of internal engines, including the applications of intelligent control technology, the fuel injection technology of diesel engine, and the embedded system design.

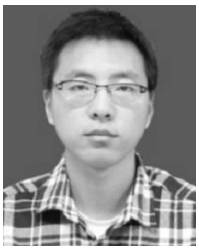

YUFEI LIU was born in Henan, China, in 1990. He received the B.S. degree in thermal energy and power engineering and the M.S. degree in power engineering from Harbin Engineering University, Harbin, China, in 2012 and 2014, respectively, where he is currently pursuing the Ph.D. degree in power engineering and engineering thermo-physics with the College of Power and Energy Engineering.

His main research interest is the application of intelligent algorithm in diesel engine, including sliding mode control and fuzzy control.

JIAN ZHANG received the B.E. and M.E. degrees from Harbin Engineering University, Harbin, China, in 2009 and 2012, respectively, and the Ph.D. degree in control science and engineering from the Harbin Institute of Technology, Harbin, in 2017. She is currently a Lecturer with the College of Power and Energy Engineering, Harbin Engineering University. Her research interests include diesel engine control, spacecraft formation coordinated control, finite-time control, and sliding mode control.

RUNZHI WANG was born in Hengyang, China, in 1990. He received the B.S. degree in thermal energy and power engineering from Harbin Engineering University, in 2013, where he is currently pursuing the Ph.D. degree in power engineering and engineering thermo-physics with the College of Power and Energy Engineering.

His main research interest is the application of intelligent algorithm in diesel engine, including model predictive control, active disturbance rejection control, and sliding mode control.